JSST
Journal of Space Science and Technology

P-ISSN: 2008-4560
E-ISSN: 2423-4516

Journal of Space Science and Technology

Vol. 19, No. 2, pp. 41-51, 2026
https://doi.org/10.22034/jsst.2025.1546
Journal Homepage: https://jsstpub.com

Original Research Paper

Design and Simulation of Radiation Shielding Using Peek Composites for Space Applications

Kavita Lalwani*, Sreedevi V V

Department of Physics, Malaviya National Institute of Technology, Jaipur, India

ARTICLE INFO

Article History:

Received 17 May 2025
Revised 03 November 2025
Accepted 05 November 2025
Available Online 09 November 2025

Keywords:

Space radiation
GCR
HZETRN
PEEK
Al
Polymer composites

ABSTRACT

Mitigation of high- energy particle radiation in space is necessary for executing long duration space missions successfully. Carbon based polymers and their composites are of huge interest in developing passive shielding techniques due to their high hydrogen content and lightweight nature. In this work, the radiation shielding properties of PEEK is evaluated in GCR free space environment using HZETRN. The total and particle wise dose equivalent is analysed in the human tissue. The variation in thermal conductivity of PEEK is also studied based on the absorbed dose results. The optimization of the shield design considers a trade-off between mechanical integrity, particularly tensile strength, and its effectiveness in attenuating radiation. The objective is to develop a multi-layered shield with PEEK-W composite and Boron Nitride (BN) in order to get adequate structural integrity and effective shielding efficacy. It is found that PEEK–tungsten (W) composite, with an additional layer of boron nitride (BN) produces 2–4% greater reduction in dose equivalent in tissue as compared to traditional materials such as aluminum. Subsequently, the total shield thickness and tungsten concentration in PEEK are optimized. The results show that a radiation shield with PEEK composite containing 40% tungsten and a total thickness of 16 g/cm2 yields the lowest dose equivalent in tissue. Further, the energy spectrum after transport through the optimized shield is studied for different particle radiations such as proton and iron present in GCR spectrum. It demonstrates the viability of PEEK-W composite as an efficient shielding material for future space exploration.

* Corresponding Author's E-mail: kavita.phy@mnit.ac.in

How to Cite this Article:
K. Lalwani, S. VV, "Design and simulation of radiation shielding using peek composites for space applications," *Journal of Space Science and Technology*, Vol. 19, No. 2, pp. 41-51, 2026, https://doi.org/10.22034/jsst.2025.1546.

COPYRIGHTS
© 2026 by the authors. Published by ARI. This article is an open access article distributed under the terms and conditions of The Creative Commons Attribution 4.0 International (CC BY 4.0)

NOMENCLATURE

GCRs	Galactic Cosmic Rays
SPEs	Solar Particle Events
SEPs	Solar Energetic Particles
CMEs	Coronal Mass Ejections
HZETRN	High charge (Z) and Energy TRaNsport
PEEK	Polyether Ether Ketone
BN	boron nitride

1. INTRODUCTION

There are a number of factors which pose a challenge for executing deep space manned missions. One of the major technological challenges is to provide adequate radiation shielding, safeguarding the health of astronauts. Space radiation also causes the spacecraft material to degrade and disrupts the electronic equipment. Hence there is a need for investigation of innovative and multifunctional materials for application in space environments. Space radiation [1] has three major sources: Galactic Cosmic Rays (GCRs), Solar Particle Events (SPEs), and trapped particles. GCRs are isotropic in their direction since they originate from high energetic sources such as supernovae well beyond the solar system. Solar Energetic Particles (SEPs) are released through solar flares and Coronal Mass Ejections (CMEs). They are sporadic and are unpredictable in nature. The radiation due to trapped particles present in Van Allen Belts are relevant only for spacecraft in Low Earth Orbit (LEO). The prominent contribution to radiation exposure during deep space missions is from the GCRs. It consists of fully ionized atomic nuclei, with charges varying from Z=1 to Z=28, that penetrate the spacecraft material and generate secondary particle radiations. Hence, in this study, only the GCR spectrum is considered for evaluating the shielding properties of materials.

Generally there are mainly two techniques for mitigation of space radiation - active and passive shielding [2]. In the method of active shielding, electromagnetic fields are used to deflect the incident particle radiations. Whereas, in passive shielding technique, we employ a material which absorbs the incident radiation. Active shielding remains largely theoretical and requires substantial advancements before it can be widely deployed. Hence, in this paper, the possibilities of improving passive shielding is explored. The challenge in developing passive shielding is that the material should be able to absorb the space radiation within the mass constraints, i.e, without increasing the total mass of the spacecraft. Conventionally, aluminum has been widely used in spacecraft as a passive shield due to its structural integrity and shielding effectiveness [3]. In this study, the shielding effectiveness of Polyether Ether Ketone (PEEK) composites is explored using HZETRN (High charge (Z) and Energy TRaNsport) [4]. PEEK is an effective option for radiation shielding in space due to its high temperature resistance, lightweight nature and low-Z composition. To improve the tensile strength of the radiation shield, a composite of PEEK with tungsten (W) is considered. To further reduce the absorbed dose, an additional layer of boron nitride (BN) is added. The total thickness of the multi-layered shield [5] composed of PEEK-W composite and boron nitride is optimized to obtain maximum dose reduction, keeping in mind the constraint on the mass of the spacecraft. Additionally, the mass percentage of tungsten in PEEK is optimized to improve the shielding effectiveness further.

2. INTERACTION OF RADIATION WITH MATTER

A passive shielding material's ability to stop incoming charged particles is described by its stopping power, which is the mean energy loss per unit distance (−dE/dx) and is given by the Bethe-Bloch Eq. [6].

$$S = -dE/dx = (4\pi e^4/m_e c^2).(Z/A).(n/\beta^2).[\ln(2m_e c^2\beta^2\gamma^2 W_{max}/I^2) - \beta^2] \quad (1)$$

where Z is the atomic number, A is the mass number, n is the electron density, $\beta = v/c$, the speed of the incoming charged particle relative to the speed of light, $\gamma = (1 - \beta^2)^{-½}$, W_{max} is the maximum energy transfer in a single collision and I is the mean excitation energy of the material.

The Bethe-Bloch equation is used to calculate how much energy a charged particle, like a proton or heavy ion, loses as it travels through a shielding material. This energy loss happens because the particle interacts with the atoms in the material, causing ionization. The amount of energy lost per unit distance is called stopping power. HZETRN uses this stopping power to find out how much energy is deposited in the material, which is then used to calculate the radiation dose - the energy deposited per unit mass. The schematic diagram describes how the radiation interacts with the shielding material and stop the radiation from reaching the human tissue within the simulation setup (Fig. 1).

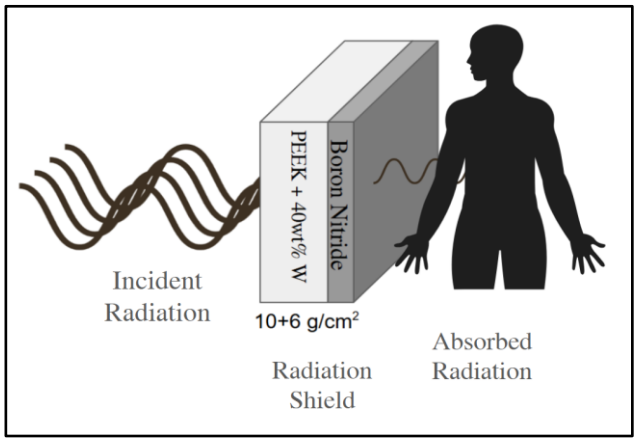

Fig. 1. Schematic diagram describing the interaction of space radiation with the shielding material and to reach the human tissue.

The physical quantities used for describing interaction of ionizing radiation with matter are:

- **Absorbed Dose (D):**

Absorbed dose measures the amount of energy deposited (E) by ionizing radiation in a unit mass (m) of a material. It is defined as,

$$D = \Delta E/\Delta m \quad (2)$$

It is expressed in units of gray (Gy), where 1 Gy =1 J/kg.

- **Dose Equivalent (H):**

Dose equivalent accounts for the biological effects of different types of radiation on human tissue. It is calculated by multiplying the absorbed dose by a radiation weighting factor (W_R), which depends on the type and energy of the radiation:

$$H = D \times W_R \quad (3)$$

Dose equivalent is expressed in units of sieverts (Sv), where 1 Sv =1 J/kg.

In this paper, in order to account for the varying biological impact of different types of radiation, dose equivalent from the radiation shield is used for studying the shielding effectiveness.

3. MATERIALS AND SIMULATION METHOD

The objective of this work is to propose a structural design of a radiation shield considering the radiation shielding effectiveness, tensile strength, temperature resistance and the possibility of outgassing of the material in space radiation environment. Materials composed of elements with low atomic numbers (particularly hydrogen) reduce the secondary fragments upon interaction with high energy radiation. Due to this reason as well as other mechanical properties, carbon based polymers are evolving as superior candidates in space radiation shielding [7,8]. PEEK draws attention due its remarkable temperature and radiation resistance and other physical and mechanical properties [9]. From literature, it was found that addition of tungsten into the PEEK matrix increases the tensile strength of the material considerably [10]. Tungsten is known for its high melting point. Additionally, to account for the generation of secondary particles, from possible nuclear fragmentation of tungsten, a layer of boron nitride is added after the PEEK-W composite [11,12]. It is expected to absorb the secondary fragments from the preceding layer. Table 1 gives the details of the shielding materials mentioned in this work. Also, this combination is non-toxic and limits out-gasing [13,14]. Both PEEK and boron nitride (BN) are listed in the NASA Outgassing Database as low-outgassing materials suitable for spacecraft use. PEEK (GSFC30151) exhibits a Total Mass Loss (TML) of 0.14%, while boron nitride (GSFC06788) [15] shows a TML of 0.12%, confirming the vacuum compatibility of the PEEK and BN.

Table 1. Details of radiation shielding materials.

S.No.	Material (Chemical Formula)	Material Density
1	Aluminium (Al)	2.7 g/cm³
2	PEEK ($C_{12}H_{12}O_3$)	1.3 g/cm³
3	Tungsten (W)	19.3 g/cm³
4	Boron Nitride (BN)	2.1 g/cm³

In the previous work [8], the primary focus was on evaluating the radiation shielding performance of polyethylene and lithium hydride-based multilayer structures. In contrast, this manuscript addresses a broader spectrum of performance metrics relevant for long-duration missions, beyond shielding effectiveness. This work places a strong emphasis on mechanical robustness, thermal conductivity, and space environment durability, recognizing that shielding materials for long-duration missions must meet multiple criteria. While the shielding performance of PEEK-W/BN is slightly lower compared to the LiH-polyethylene system, it offers significant mechanical strength and thermal stability [10], making it more viable for structural integration and extended missions. A comparative table summarizing the key differences between the LiH+polyethylene system [8] and the current PEEK-W+BN system is discussed in Table 2.

Table 2. Comparison between the properties of LiH+Polyethylene and PEEK-W+BN configurations.

LiH + Polyethylene	PEEK-W+BN
An improved shielding effectiveness of 54.9% when compared to aluminum.	The shielding effectiveness is greater than aluminum by 2 - 4%.
Polyethylene provides the required structural integrity to the shield [16].	The tungsten added to the PEEK matrix improves the tensile strength of the shield significantly [10].
Not thermally stable [17].	PEEK and W exhibit excellent thermal stability [9].
Prone to outgassing [18].	Very low chances of outgassing [13,14].

In the previous study [8], one of the key objectives was to perform a cross-validation of radiation dose calculations using both HZETRN and OLTARIS. The comparison confirmed that the results from both tools were in close agreement for the types of shielding scenarios and particle environments considered. The objective of the present study, however, is not to revalidate the tools, but to propose a structural design of a radiation shield considering the radiation shielding effectiveness, tensile strength, temperature resistance and the possibility of outgassing of the material in space radiation environment. Given that the computational validation of HZETRN against OLTARIS was already performed and published in our previous study [8], where the results were in agreement, repeating that comparison here would be redundant and would not provide new insights. Therefore, for clarity and efficiency, we have limited the current analysis to HZETRN. HZETRN is used to simulate the materials, which is a deterministic transport code provided by NASA [19]. The HZETRN code is a deterministic model developed by NASA to simulate the transport of space radiation. It solves the time-independent, linear Boltzmann equation numerically. It consists of two modules - cross section and transport. The cross section module calculates the stopping power, total reaction cross section and fragmentation cross section for any particle interaction. This is where the cross section databases for each material is generated and stored. The transport module simulates the space radiation transport through the radiation shield.

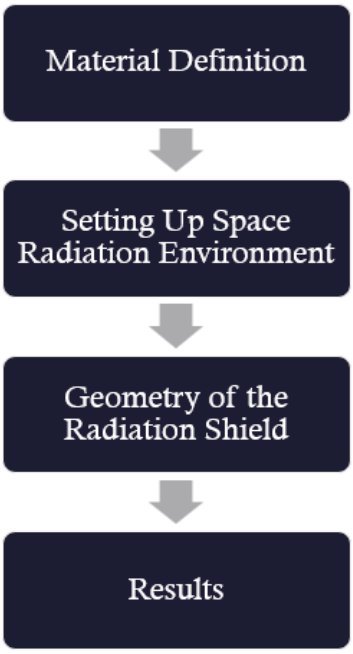

Fig. 2. Flowchart of simulation in HZETRN.

Figure 2 shows the various steps involved in executing the simulation using HZETRN such as defining the material composition, radiation environment and geometry of the radiation shield. The first step is to create the cross section database for the shielding materials. For this the chemical composition and density of each material has to be specified. This is done in the cross sections module. The next step is to define the radiation environment by defining the input flux. The code supports the simulation of GCR, SPE, LEO and custom boundary conditions. In this study, only the GCR environment is considered. The GCR spectra were generated using the BON-2014 (Badhwar–O'Neill 2014) [20] model, which is implemented in HZETRN. This model includes all ion species from hydrogen (Z = 1) up to nickel (Z = 28). The solar modulation parameter ('phi' in units of megavolts) which accounts for the solar activity at that point in time is chosen as φ = 475 MV to represent solar minimum conditions. It denotes the solar modulation potential in the force-field approximation, representing the average energy loss (per unit charge) that galactic cosmic ray particles undergo while propagating through the heliosphere under solar minimum conditions. The value φ = 475 MV was chosen because it represents a commonly used parameterization of solar minimum conditions in galactic cosmic ray (GCR) transport models. The solar modulation potential varies typically between ~400–600 MV during solar minimum and ~1000–1600 MV during solar maximum. A φ of 475 MV corresponds to a period of low solar activity when GCR fluxes are near their maximum intensity [21].

The final step in running the simulation is to define the geometry of the radiation shield. The basic geometry can be either semi- infinite slab, sphere or user defined configuration with any number of materials/layers in any order. The thickness of each layer has to be specified. Also, the response material in which the dose is calculated also needs to be chosen. This study analyses the dose equivalent calculated in tissue applying the ICRP 60 [22] quality factor, for a one-day mission. The primary objective of this work is to assess the role of shield composition in GCR attenuation for astronaut protection and hence is limited to dose equivalent in tissue. Although space radiation also impacts non-biological materials (electronics, polymers, structures), these require different metrics (e.g., total ionizing dose, displacement damage) and are outside the scope of this study. Since dose scales linearly with mission duration, the reported 2–4% reduction(section 4.5) is independent of exposure time. Similarly, changes in solar modulation or mission environment alter absolute dose values but only modestly affect the relative reduction, which is composition-driven. Semi infinite slab geometry is used to simulate the radiation shield. The semi-infinite slab geometry highlights intrinsic material behavior; while realistic spacecraft geometries may shift absolute values, the composition-driven relative reduction is expected to remain of the same order.

4. RESULTS

In this section, the radiation shielding properties such as total and particle wise dose equivalent from a radiation shield made of PEEK are studied. Further, the variation in thermal conductivity with depth of PEEK is computed. The results are compared with that of one of the traditional shielding materials, Aluminum. The particle wise energy spectrum after

transport through the shield is also analysed. Subsequently, the shielding properties of a composite material formed by adding tungsten into PEEK matrix along with a layer of boron nitride is studied. Further, the mass percentage of tungsten in PEEK and the total thickness of the radiation shield is optimized.

4.1 Dose Equivalent from Aluminium and PEEK

In order to understand the shielding properties of PEEK material, it is necessary to study its properties in the space radiation environment. Here, the dose equivalent of PEEK is simulated and studied in a free space GCR environment at each depth of a 16 g/cm^2 thick shield. The results are compared with the traditional shielding material (Aluminum) and are shown in Fig. 3.

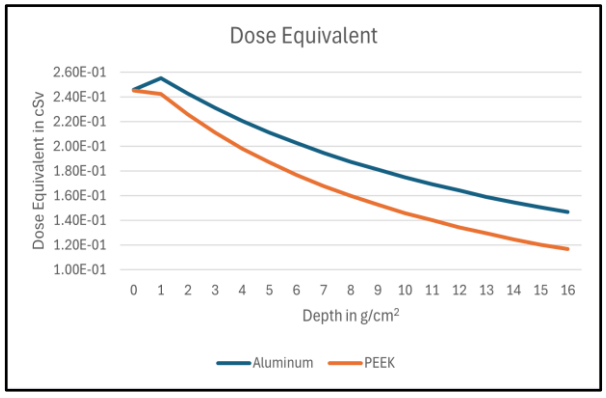

Fig. 3. Variation of dose equivalent with depth of PEEK and Aluminum

It can be seen that at all depths, PEEK produces less dose equivalent than Aluminum. This is due to the high hydrogen content and low atomic number of elements which constitute PEEK. At maximum depth, there is a decrease of 20.4% in the dose equivalent value.

4.2 Particle Wise Dose Equivalent from PEEK and Aluminum

The variation in dose equivalent from proton and iron with depth are studied separately. Proton has the highest flux in the GCR spectrum and can be also produced due to secondary interactions. Iron is chosen to represent heavy ions in the GCR spectra. Fig. 4 shows the results of variation of dose equivalent from proton and iron with depth for Aluminum and PEEK. It can be seen that the dose equivalent from protons increases with depth. This is due to the production of protons from secondary interactions. Iron is rarely produced as a secondary particle whereas nucleus–nucleus collisions produce lighter fragments such as protons. Heavy ions (HZE) lose energy and are attenuated as they traverse material, so the dose contribution from surviving primary Fe nuclei decreases with depth. Simultaneously, the charged fragments (notably protons) may accumulate and deposit dose at greater depths, producing a fragmentation "buildup" in the total depth-dose. We can clearly see from the fig. that in both the cases PEEK has lower value of dose equivalent than Aluminum.

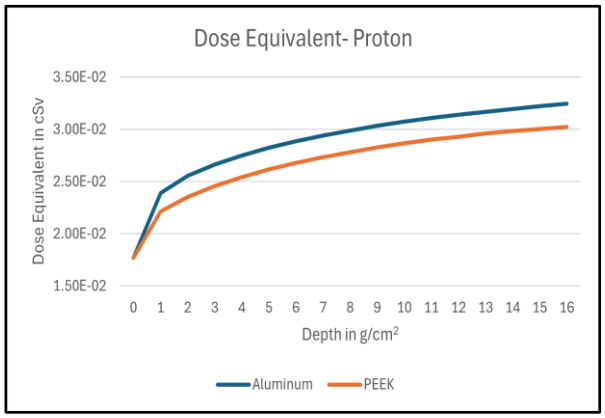

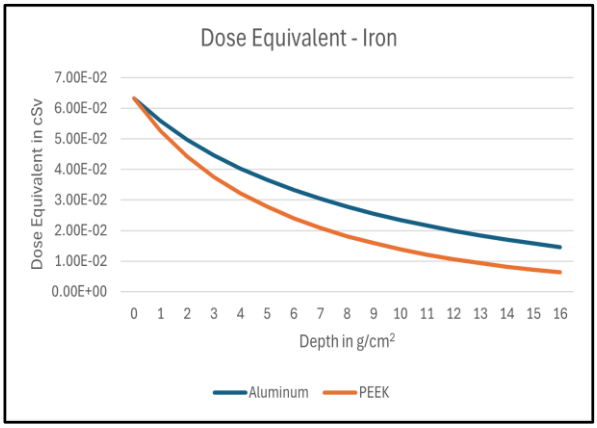

Fig. 4. Variation of dose equivalent from proton (left) and Iron (right) with depth of Aluminum and PEEK.

4.3 Thermal Conductivity of PEEK and Aluminium

In order to understand the temperature resistance of PEEK, the variation of thermal conductivity with depth is calculated from absorbed dose. The thermal conductivity of Aluminum and PEEK are modelled through the relation,

$$K = K_0 \exp(-\alpha D) \quad (4)$$

where K_0 is the initial thermal conductivity, α is the degradation sensitivity and D is the absorbed dose. This model is consistent with experimental observations reported for irradiated ceramics [23]. The variation of thermal conductivity with depth of Aluminum and PEEK are shown in Fig. 5.

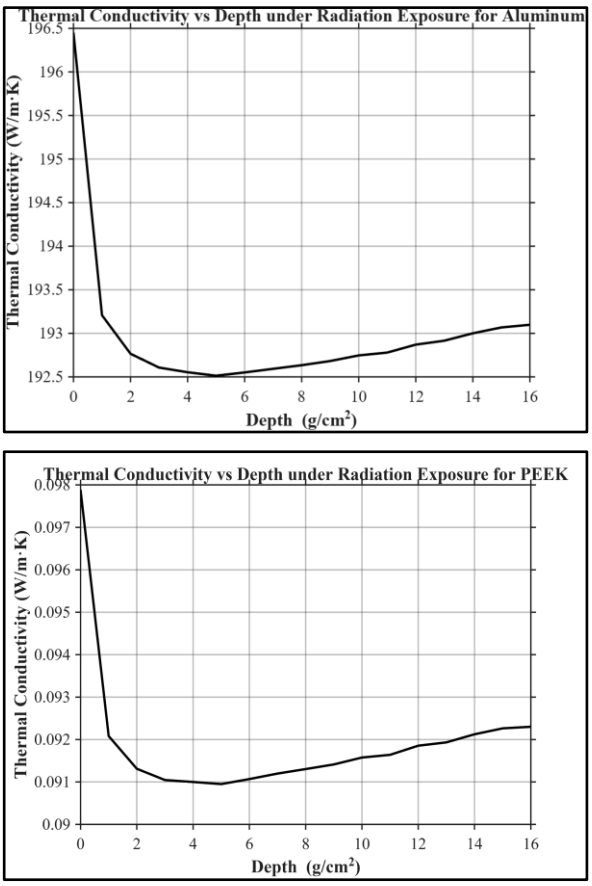

Fig. 5. Variation of thermal conductivity with depth of Aluminum (left) and PEEK (right) in GCR environment.

This computation is done using MATLAB [24] using the absorbed dose results obtained from HZETRN. All GCR components were simulated for the computation of absorbed dose. As polymers are more sensitive to radiation damage than metals, the value of α is chosen as 5 cGy^{-1} for Aluminum and 25 cGy^{-1} for PEEK. The value of K_0 for Aluminum and PEEK is 237 W/m.K [25] and 0.25 W/m.K [26] respectively. It can be seen that the thermal conductivity of PEEK is much less than that of Aluminum. As the space environment involves vast temperature variations, ranging from over +120 °C in direct sunlight to below −150 °C in shadow [27], PEEK's high thermal stability (up to ~260 °C) [28] and resistance to degradation make it highly suitable for maintaining structural integrity under such extreme thermal conditions. It shows that PEEK is a highly temperature resistant material which is often desired in extreme conditions in the space radiation environments. In this work, the degradation of thermal conductivity was modeled as a function of absorbed dose, which provides a convenient macroscopic measure of radiation exposure. This approach does not explicitly account for track-structure effects caused by high-LET heavy ions in GCR, which are known to induce disproportionate damage in polymers through localized bond scission and defect formation. As a result, the model may underestimate localized degradation mechanisms driven by heavy-ion tracks. Nevertheless, using absorbed dose as the primary parameter enables a first-order assessment of thermal property changes and offers practical applicability for comparative shield studies.

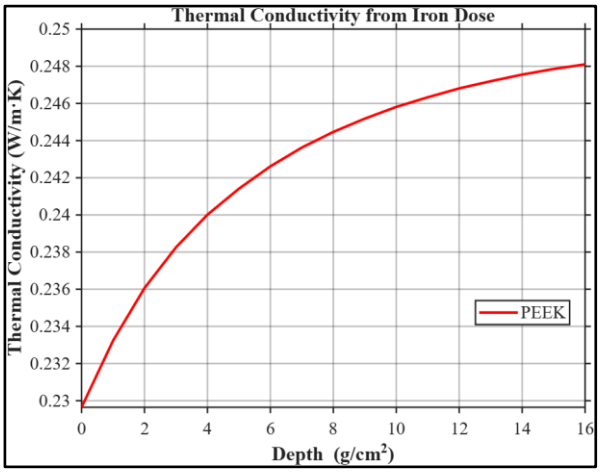

Fig. 6. Thermal conductivity as a function of depth modelled using absorbed dose from iron nuclei.

The thermal conductivity of PEEK is modelled using the absorbed dose from iron ions alone to represent the contribution of heavy ions. The results are shown in Fig. 6. For Fe ions, the absorbed dose decreases with depth due to nuclear fragmentation and energy loss. Since the thermal conductivity degradation model is dose-dependent, this results in

larger reductions at the material surface and a gradual recovery of K toward the unirradiated value with depth. Thus, the apparent increase in conductivity with depth reflects the reduced local dose contribution from heavy ions rather than an intrinsic improvement of the material.

4.4 Energy Spectrum After Transport

The energy spectrum of proton and iron after transport through a 16 g/cm^2 thick radiation shield of PEEK is studied. The results are shown in Fig. 7.

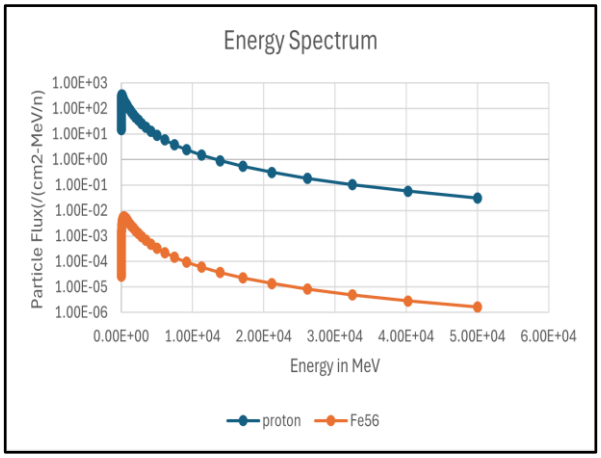

Fig. 7. Energy spectrum after transport through radiation shield composed of PEEK.

The particle flux decreases at higher energies. As mentioned before, the relative high values of proton flux is due to the production of protons from secondary interactions.

4.5 Dose Equivalent From PEEK Composite and Aluminum

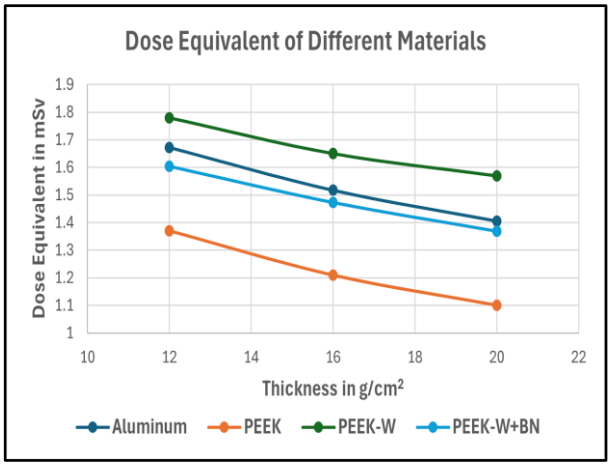

Fig. 8. Dose equivalent as a function of thickness of Aluminum & PEEK composite.

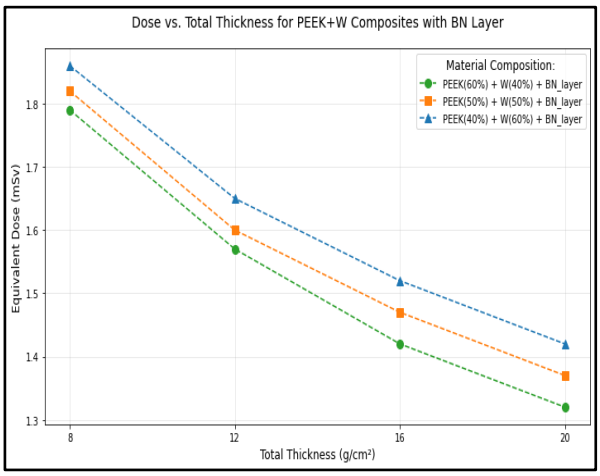

Fig. 9. Dose equivalent as a function thickness for PEEK with 40%,50% and 60% of tungsten.

In order to improve the tensile strength of the radiation shield, a PEEK composite with 50 wt% of tungsten is considered [10]. An additional layer of boron nitride is simulated which is expected to absorb neutrons generated by nuclear fragmentation of tungsten. The dose equivalent of the new configuration is computed by varying the total thickness of the shield as 12 g/cm^2, 16 g/cm^2 and 20 g/cm^2 where the thickness of BN layer is 4 g/cm^2, 6 g/cm^2 and 8 g/cm^2 respectively. The results on dose equivalent are shown in fig. 8. It clearly shows the difference between pure PEEK and PEEK-W+BN combination where the dose equivalent is reduced by 10.7% with PEEK-W+BN configuration as compared to PEEK-W. The PEEK-W composite along with the BN layer demonstrates superior shielding performance compared to aluminum across all the thicknesses. At a total thickness of 16 g/cm^2, the proposed composite achieves a 2.8% reduction in dose equivalent relative to Aluminum, highlighting its enhanced effectiveness in radiation protection. 16 g/cm^2 is the optimum thickness for the radiation shield considering the shielding effectiveness and mass constraints. Increasing shielding thickness beyond 16 g/cm^2 becomes increasingly impractical due to strict spacecraft mass constraints, especially in crewed missions [29]. Therefore, the chosen thickness reflects a practical compromise between shielding performance and payload limitations.

4.6 Mass Percentage Optimization of Tungsten in the composite shield

For the optimization of mass percentage of tungsten in PEEK, the dose equivalent as a function

of thickness for 40 wt%, 50 wt% and 60 wt% of tungsten is computed. The corresponding results are

shown in fig. 9. From the results, it can be seen that as the percentage composition of tungsten increases, the dose equivalent increases. This is possibly due to the nuclear fragmentation of tungsten. 40% of tungsten can be considered as optimum composition since it provides better shielding effectiveness.

4.7 Particle Wise Dose Equivalent of Optimized Radiation Shield (PEEK-W + BN)

The particle-wise dose equivalent from the optimized radiation shield is shown fig 10.

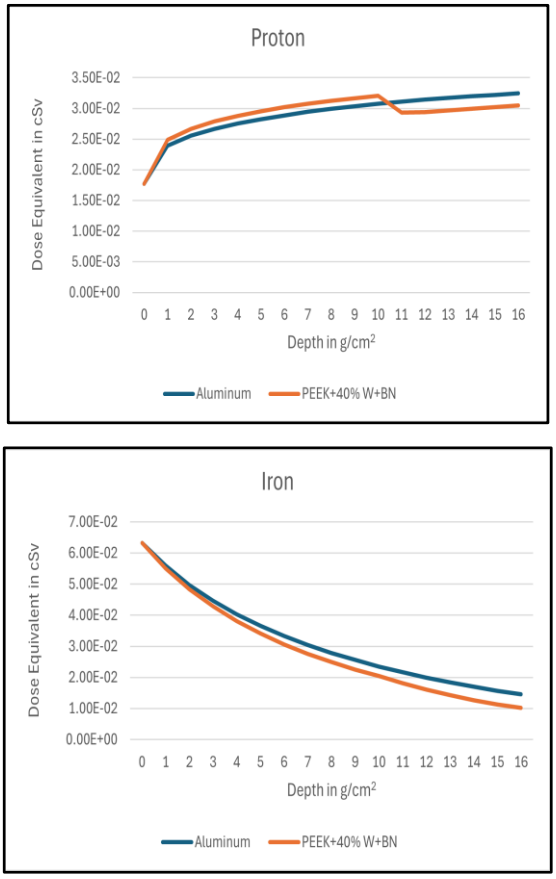

Fig. 10. Comparison of dose equivalent from proton (left) and iron (right) between Aluminum and PEEK+W composite with BN.

From fig. 10, it can be seen that PEEK, upon addition of tungsten, gives higher dose equivalent than Aluminum. This is due to the increased possibility of nuclear fragmentation from tungsten. The second layer of the shield, made of boron nitride is able to absorb the extra secondary particles generated and reduce the total dose equivalent. Thus, the optimized shield still shows better dose reduction than Aluminum. Alternative layer arrangements (e.g., placing BN before or mixing it with PEEK-W) were not considered, as such arrangements would reduce the BN layer's exposure to secondary neutrons originating from tungsten. This would not effectively fulfill the primary objective of absorbing secondary neutrons generated from tungsten fragmentation.

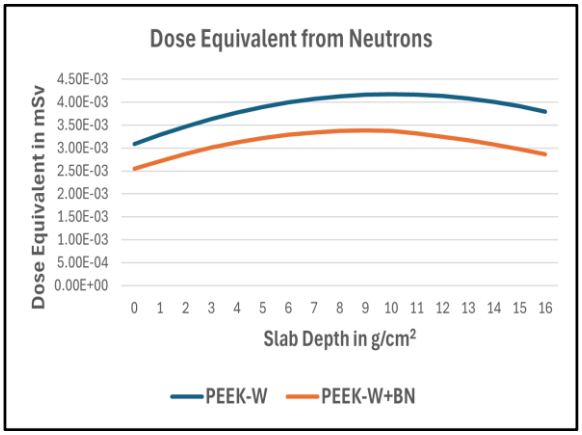

Fig. 11. Neutron dose equivalent in PEEK-W and PEEK-W+BN configurations.

In order to show that the BN layer absorbs neutrons generated from tungsten fragmentation, dose equivalent as a function of depth is shown for PEEK-W+BN and it is compared with PEEK-W configuration in fig. 11. At total thickness, a reduction of 27 % in dose equivalent is achieved by the addition of the BN layer. This reduction confirms the absorption of secondary neutrons generated from tungsten fragmentation. Neutrons which are neutral particles do not undergo coulomb interaction and hence penetrate deep inside the target material. However the B-10 isotope of Boron in BN undergoes neutron capture reaction, reducing the overall dose equivalent.

5. SUMMARY

This study presents the evaluation of PEEK as a structural as well as radiation shielding material for space applications. The results indicate the superiority of PEEK when compared to traditional materials like aluminum. Further shielding effectiveness of a radiation shield with modified structure using PEEK-W composite and BN is

evaluated. Tungsten improves the tensile strength of the shield. But the addition of tungsten increases the absorbed dose and to account for this BN is added as a separate layer. The modified shield still outperforms Aluminum by showing 2-4% better dose reduction. Further the thickness of various layers of the shield and the mass percentage of tungsten in PEEK are optimized. It has been found that a configuration with 16 g/cm² of PEEK-W composite and BN layer with 40% of W in PEEK is the optimal design.

6. ACKNOWLEDGEMENTS

We are grateful for MNIT Jaipur to support this work. We extend our gratitude to the HZETRN transport code provided by NASA.

CONFLICTS OF INTERESTS

No conflict of interest has been expressed by the authors.

REFERENCES

[1] G. A. Nelson, "Space radiation and human exposures, a primer," *Radiation Research*, vol. 185, no. 4, pp. 349–358, 2016, https://doi.org/10.1667/RR14311.1.

[2] P. Spillantini *et al.*, "Shielding from cosmic radiation for interplanetary missions: Active and passive methods, *Radiation Measurements*, vol. 42, no. 1, pp. 14-23, 2007, https://doi.org/10.1016/j.radmeas.2006.04.028.

[3] N. Masayuki and S. Kodaira, "Considerations for practical dose equivalent assessment of space radiation and exposure risk reduction in deep space," *Scientific Reports*, vol. 12, 2022, Art. no. 13617, https://doi.org/10.1038/s41598-022-17079-1.

[4] J. W. Wilson *et al.*, "Description of a free-space ion and nucleon transport and shielding computer program," NASA, Tech. Rep. TP-3495, 1995.

[5] A. Gohel and R. Makwana, "Multi-layered shielding materials for high energy space radiation," *Radiation Physics and Chemistry*, vol. 197, 2022, Art. no. 110131, https://doi.org/10.1016/j.radphyschem.2022.110131.

[6] F. Salvat, "Bethe stopping-power formula and its corrections," *Physical Review A*, vol. 106, 2022, Art. no. 032809, https://doi.org/10.1103/PhysRevA.106.032809.

[7] E. Toto, L. Lambertini, S. Laurenzi, and M. G. Santonicola, "Recent advances and challenges in polymer-based materials for space radiation shielding," *Polymers*, vol. 16, no. 3, 2024, Art. no. 382, https://doi.org/10.3390/polym16030382.

[8] S. V. V and K. Lalwani, "Effectiveness of multi-layered radiation shields constructed from polyethylene and metal hydrides using HZETRN and OLTARIS for space applications," vol. 18, Special Issue, pp. 26-33, 2025, https://doi.org/10.22034/jsst.2025.1520.

[9] M. Rinaldi, M. Ferrara, L. Pigliaru, C. Allegranza, and F. Nanni, "Additive manufacturing of polyether ether ketone-based composites for space application: A mini-review," *CEAS Space Journal*, vol. 15, no. 1, pp. 77-87, 2023, https://doi.org/10.1007/s12567-021-00401-4.

[10] Y. Wu, Y. Cao. Y. Wu, and D. Li, "Mechanical properties and gamma-ray shielding performance of 3D-printed poly-ether-ether-ketone/tungsten composites," *Materials*, vol. 13, no. 20, 2020, Art. no. 4475, https://doi.org/10.3390/ma13204475.

[11] E. Cheraghi, S. Chen, and J. TW Yeow, "Boron nitride-based nanomaterials for radiation shielding: A review," *IEEE Nanotechnology Magazine*, vol. 15, no. 3, pp. 8-17, 2021, https://doi.org/10.1109/MNANO.2021.3066390.

[12] S. Kim, Y. Ahn, S. Ho Song, and D. Lee, "Tungsten nanoparticle anchoring on boron nitride nanosheet-based polymer nanocomposites for complex radiation shielding," *Composites Science and Technology*, vol. 221, 2022, Art. no. 109353, https://doi.org/10.1016/j.compscitech.2022.109353.

[13] T. J. Patrick, "Outgassing and the choice of materials for space instrumentation," *Vacuum*, vol. 23, no. 11, pp. 411-413, 1973, https://doi.org/10.1016/0042-207X(73)92531-1.

[14] R. Pastore *et al.*, "Outgassing effect in polymeric composites exposed to space environment thermal-vacuum conditions," *Acta Astronautica*, vol. 170, pp. 466-471, 2020, https://doi.org/10.1016/j.actaastro.2020.02.019.

[15] NASA. "Outgassing database." [Online]. Available: https://etd.gsfc.nasa.gov/capabilities/outgassing-database/

[16] J. H. Cha, S. Kumar Sarath Kumar, J. E. Noh. J. S. Choi. Y. Kim, and C. G. Kim, "Ultra-high-molecular-weight polyethylene/hydrogen-rich benzoxazine composite with improved interlaminar shear strength for cosmic radiation shielding and space environment applications," *Composite Structures*, vol. 300, 2022, Art. no. 116157, https://doi.org/10.1016/j.compstruct.2022.116157.

[17] M. Gardette *et al.*, "Photo-and thermal-oxidation of polyethylene: Comparison of mechanisms and influence of unsaturation content," *Polymer Degradation and Stability*, vol. 98, no. 11, pp. 2383-2390, 2013,

https://doi.org/10.1016/j.polymdegradstab.2013.07.017.

[18] L. N. Dinh *et al*., "Vacuum outgassing of high density polyethylene," *Journal of Vacuum Science & Technology A*, vol. 27, no. 2, pp. 376-380, 2009, https://doi.org/10.1116/1.3085719.

[19] NASA. [Online]. Available: https://www.nasa.gov/

[20] P. M. O'Neill, S. Golge, and T. C. Slaba, "Badhwar-O'Neill 2014 galactic cosmic ray flux model description," NASA, Tech. Rep. JSC-CN-32930, 2015.

[21] L. J. Gleeson and W. I. Axford, "Solar modulation of galactic cosmic rays," *Astrophysical Journal,* vol. 154, 1968, Art. no. 1011.

[22] A. V. Sannikov and E. N. Savitskaya, "Ambient dose equivalent conversion factors for high energy neutrons based on the ICRP 60 recommendations," *Radiation Protection Dosimetry*, vol. 70, no. 1-4, pp. 383–386, 1997, https://doi.org/10.1093/oxfordjournals.rpd.a031982.

[23] W. Knappe and O. Yamamoto, "Effects of crosslinking and chain degradation on the thermal conductivity of polymers," *Kolloid-Zeitschrift und Zeitschrift für Polymere*, vol. 240, no. 1, pp. 775-783, 1970, https://doi.org/10.1007/BF02160074.

[24] D. M. Etter, D. C. Kuncicky, and D. W. Hull, *Introduction to MATLAB 6*, 2rd ed. Hoboken, NJ, USA: Prentice Hall, 2004.

[25] HTS-ALU. "Thermal conductivity of Aluminum." https://hts-alu.com/thermal-conductivity-of-aluminium/

[26] M. Rinaldi, F. Cecchini, L. Pigliaru, T. Ghidini, F. Lumaca, and F. Nanni, "Additive manufacturing of polyether ether ketone (PEEK) for space applications: A nanosat polymeric structure," *Polymers*, vol. 13, no. 1, 2020, Art. no. 11, https://doi.org/10.3390/polym13010011.

[27] D. G. Gilmore, *Spacecraft Thermal Control Handbook: Cryogenics,* Vol. 2, AIAA, 2002.

[28] P. Patel, T. Richard Hull, R. W. McCabe, D. Flath, J. Grasmeder, and M. Percy, "Mechanism of thermal decomposition of poly (ether ether ketone)(PEEK) from a review of decomposition studies," *Polymer Degradation and Stability*, vol. 95, no.5, pp. 709-718, 2010, 709-718. https://doi.org/10.1016/j.polymdegradstab.2010.01.024.

[29] f. Horst, D. Boscolo. M. Durante, F. Luoni, C. Schuy, and U. Weber, "Thick shielding against galactic cosmic radiation: A Monte Carlo study with focus on the role of secondary neutrons," *Life Sciences in Space Research*, vol. 33, pp. 58-68, 2022, https://doi.org/10.1016/j.lssr.2022.03.003.